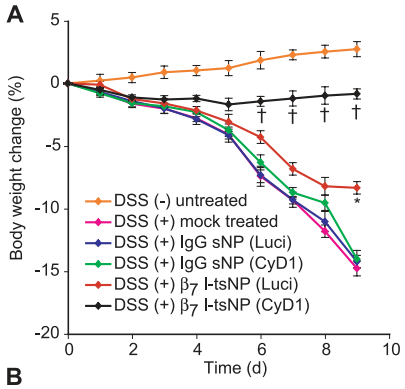

B

Mice treatment	HCT (mean ± SEM) (%)
DSS (-) untreated	57.2 ± 0.9
DSS (+) mock treated	40.4 ± 3.4
DSS (+) IgG sNP (Luci)	39.9 ± 3.9
DSS (+) IgG sNP (CyD1)	43.5 ± 2.6
DSS (+) β_7 I-tsNP (Luci)	45.7 ± 7.3
DSS (+) β_7 I-tsNP (CyD1)	53.2 ± 1.7 †

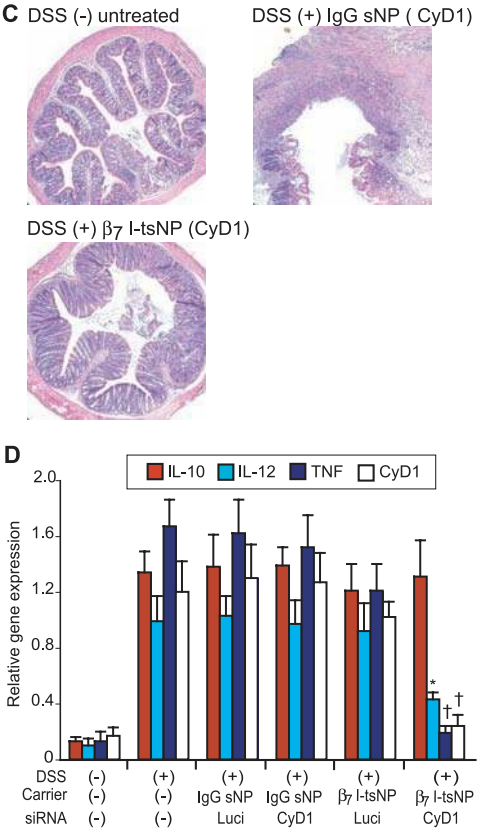

Fig. 4. Cyclin-D1–siRNA delivered by β_7 I-tsNP alleviated intestinal inflammation in DSS-induced colitis. Mice were intravenously administered CyD1- or luciferase (Luci)-siRNAs (2.5 mg/kg) entrapped in either β_7 I-tsNPs or IgG-sNPs, or naked CyD1-siRNA (2.5 mg/kg) at days 0, 2, 4, and 6 (a total of six mice per group in three independent experiments). (**A**) Change in body weight. (**B**) Hematocrit (HCT) measured at day 9. (**C**) Representative histology at day 9 (hematoxylin and eosin staining, magnification ×100). (**D**) mRNA expression of CyD1 and cytokines in the gut. mRNA expression was measured by qRT-PCR with homogenized colon samples harvested at day 9. (A), (B), and (D) Data are expressed as the mean ± SEM of three independent experiments. *$P < 0.05$, †$P < 0.01$ versus mock-treated mice with DSS-induced colitis.

body targets for both delivery and uptake of tsNPs. Thus, the I-tsNP approach may have broad applications not only for in vivo drug target validation, but also for potential therapies that are not limited to leukocytes or inflammatory settings.

References and Notes

1. E. Iorns, C. J. Lord, N. Turner, A. Ashworth, *Nat. Rev. Drug Discov.* **6**, 556 (2007).
2. D. W. Stacey, *Curr. Opin. Cell Biol.* **15**, 158 (2003).
3. M. Fu, C. Wang, Z. Li, T. Sakamaki, R. G. Pestell, *Endocrinology* **145**, 5439 (2004).
4. R. Yang, W. Bie, A. Haegebarth, A. L. Tyner, *Cell Cycle* **5**, 180 (2006).
5. H. van Dekken *et al.*, *Acta Histochem.* **109**, 266 (2007).
6. M. A. Behlke, *Mol. Ther.* **13**, 644 (2006).
7. D. M. Dykxhoorn, J. Lieberman, *Annu. Rev. Biomed. Eng.* **8**, 377 (2006).
8. D. Peer, P. Zhu, C. V. Carman, J. Lieberman, M. Shimaoka, *Proc. Natl. Acad. Sci. U.S.A.* **104**, 4095 (2007).
9. Materials and methods are available as supporting material on *Science* Online.
10. C. R. Dass, *J. Mol. Med.* **82**, 579 (2004).
11. D. Peer, A. Florentin, R. Margalit, *Biochim. Biophys. Acta* **1612**, 76 (2003).
12. D. P. Andrew *et al.*, *J. Immunol.* **153**, 3847 (1994).
13. S. K. Shaw, M. B. Brenner, *Semin. Immunol.* **7**, 335 (1995).
14. F. L. Sorgi, S. Bhattacharya, L. Huang, *Gene Ther.* **4**, 961 (1997).
15. S. D. Li, L. Huang, *Mol. Pharm.* **3**, 579 (2006).
16. J. O. Lindsay, A. Sandison, P. Cohen, F. M. Brennan, H. J. Hodgson, *Dig. Dis. Sci.* **49**, 1327 (2004).
17. J. Soutschek *et al.*, *Nature* **432**, 173 (2004).
18. D. V. Morrissey *et al.*, *Nat. Biotechnol.* **23**, 1002 (2005).
19. R. M. Schiffelers *et al.*, *Nucleic Acids Res.* **32**, e149 (2004).
20. E. Song *et al.*, *Nat. Biotechnol.* **23**, 709 (2005).
21. F. Takeshita *et al.*, *Proc. Natl. Acad. Sci. U.S.A.* **102**, 12177 (2005).
22. J. D. Heidel *et al.*, *Proc. Natl. Acad. Sci. U.S.A.* **104**, 5715 (2007).

23. We thank J. Lieberman for critically reading manuscript and discussion; R. Margalit, R. S. Langer, and P. Sicinski for discussions; and Y. Imai, A. Zur, P. Sage, and R. Yoo for technical assistance. D.P. is supported by the Dorot Foundation and Pfizer Inc. Y.M. is supported by the Uehara Memorial Foundation. This work was supported by the Arthritis Foundation (C.V.C.) and NIH grants HL048675 and AI63421 (M.S.).

Supporting Online Material

www.sciencemag.org/cgi/content/full/319/5863/627/DC1
Materials and Methods
Figs. S1 to S12
Tables S1 to S3
References

29 August 2007; accepted 18 December 2007
10.1126/science.1149859

Direct Observation of Hierarchical Folding in Single Riboswitch Aptamers

William J. Greenleaf,[1*] Kirsten L. Frieda,[2] Daniel A. N. Foster,[4] Michael T. Woodside,[4,5*†] Steven M. Block[1,3†]

Riboswitches regulate genes through structural changes in ligand-binding RNA aptamers. With the use of an optical-trapping assay based on in situ transcription by a molecule of RNA polymerase, single nascent RNAs containing *pbuE* adenine riboswitch aptamers were unfolded and refolded. Multiple folding states were characterized by means of both force-extension curves and folding trajectories under constant force by measuring the molecular contour length, kinetics, and energetics with and without adenine. Distinct folding steps correlated with the formation of key secondary or tertiary structures and with ligand binding. Adenine-induced stabilization of the weakest helix in the aptamer, the mechanical switch underlying regulatory action, was observed directly. These results provide an integrated view of hierarchical folding in an aptamer, demonstrating how complex folding can be resolved into constituent parts, and supply further insights into tertiary structure formation.

Riboswitches are elements of mRNA that regulate gene expression through ligand-induced changes in mRNA secondary or tertiary structure (*1*, *2*). This regulation is accomplished through the binding of a small metabolite to an aptamer in the 5′-untranslated region of the mRNA, which causes conformational changes that alter the expression of downstream genes. Riboswitch-dependent regulatory processes depend crucially on the properties of aptamer folding; the kinetics and thermodynamics of folding are therefore of central importance for understanding function.

Among the simplest riboswitches are those regulating purine metabolism, which have aptamers with "tuning fork" structures (*3*, *4*) that bind ligands at a specific residue in a pocket formed by a three-helix junction. The junction is thought to be preorganized by numerous tertiary contacts, including interactions between two hairpin loops, but the binding pocket itself is likely stabilized only upon ligand binding (*4*–*10*). Ligand binding also stabilizes a nearby helix (*3*–*5*), sequestering residues that would otherwise participate in an alternate structure affecting gene expression (e.g., terminator or anti-terminator hairpins, ribosome binding sequences). Features such as ligand specificity (*6*, *11*) and its structural basis (*6*, *7*), the rates and energies for ligand binding and dissociation (*12*), the kinetics of loop-loop formation (*10*), and the interplay of structural preorganization and induced fit (*7*–*9*) have recently been investigated. These studies, how-

Downloaded from www.sciencemag.org on March 19, 2008

ever, focused on isolated steps in folding, typically using ligand analogs or investigating aptamers from different organisms. Here we obtain, from a single set of measurements, an integrated picture of secondary and tertiary structure formation, as well as ligand binding, in the aptamer of the *pbuE* adenine riboswitch from *Bacillus subtilis*, by observing folding and unfolding trajectories of individual molecules subjected to controlled loads in a high-resolution, dual-trap optical tweezers apparatus (*13*).

Single-molecule force spectroscopy, which measures the extension of a molecule as it unfolds and refolds under tension, furnishes a tool for probing structural transitions: Extension changes can be related to the number of nucleotides involved in folding. Furthermore, the effects of force on reaction equilibria and kinetics allow the shapes of the folding landscapes to be determined in detail (*14*–*16*). The complete folding process, starting from a fully unfolded state (not usually probed in conventional RNA folding studies), can also be observed. This initial configuration is especially relevant to riboswitches, because aptamers fold cotranscriptionally from an initially unstructured state. Because of the tight coupling between folding and transcription, the assay was designed to measure folding of mRNA transcribed in situ (*17*). A single *Escherichia coli* RNA polymerase (RNAP) molecule, transcriptionally stalled downstream of the promoter region on a DNA template (Fig. 1A), was attached to a bead held in one optical trap (Fig. 1B). The 29-nucleotide (nt) initial RNA transcript emerging from the RNAP was hybridized to the complementary cohesive end of a 3-kb double-stranded DNA (dsDNA) "handle" attached to a bead held in the other trap, creating a "dumbbell" geometry that allowed forces to be applied between the RNAP and the 5′ end of the RNA (*18*). Force-extension curves (FECs), showing the molecular extension measured as a function of force as the traps were moved apart at a constant rate, confirmed that this initial transcript was unstructured (Fig. 1C).

After constructing the dumbbells, transcription was restarted by introducing nucleoside triphosphates. The DNA template coded for the *pbuE* adenine riboswitch aptamer downstream of the initial transcript (Fig. 1A). Once the aptamer sequence was transcribed, RNAP was prevented from further elongation by a roadblock consisting of a streptavidin molecule bound to a 5′-terminal biotin label on the template (Fig. 1D). FECs measured immediately after aptamer transcription (Fig. 1E) revealed a characteristic series of sawtooth features that arise from contour length increases as specific structural elements unfold (*19*). In the absence of adenine, two small unfolding events were typically observed (Fig. 1E, black). These features are produced by the unfolding of the two stable hairpins in the secondary structure, P3 and P2 (Fig. 1E, inset). The interactions that underpin tertiary structure by holding these hairpin loops together and structuring the binding pocket in the triple-helix junction are present only transiently in the absence of adenine (*5*, *8*, *10*). The contour length changes associated with these features, 17 ± 2 nt (P3) and 22 ± 2 nt (P2), are consistent with the values expected for these hairpins (19 and 21 nt, respectively) (*18*). In the presence of adenine, some FECs were identical to those observed in its absence, indicating in these cases that adenine was not bound to the aptamer. More commonly, however, larger unfolding distances at higher forces were observed, corresponding to adenine-induced stabilization of the folded structure. In the latter case, the aptamer usually unfolded cooperatively in a single event (Fig. 1E, blue), but sometimes through an intermediate state (Fig. 1E, red).

Unfolding from the fully folded state was analyzed in more detail by collecting multiple FECs from the same molecule. Overlaying 800 FECs shows that the aptamer unfolds over a wide distribution of forces (Fig. 2A), as expected for a nonequilibrium measurement (*20*). Three states were clearly seen: the folded and unfolded states, and an intermediate state. We fit the FECs with two worm-like chains (WLCs) in series: one for the dsDNA handle (*21*) and the other for the single-stranded RNA (*22*), assuming a contour length of 0.59 nm/nt for RNA (*23*). When the aptamer unfolded fully, 62 ± 1 nt were released (*18*), in agreement with the 63-nt aptamer length. The intermediate state is 23 ± 1 nt shorter than the unfolded state, suggesting that it corresponds to a folded 21-nt P2 helix. The equilibrium free energy of the aptamer, computed by the method of Jarzynski (*24*, *25*) from the nonequilibrium work done to unfold it (fig. S2), is 18 ± 2 kcal/mol (*18*). For comparison, the free energy predicted for the secondary structure in Fig. 1E is only ~12 ± 1 kcal/mol (*10*), indicating that tertiary contacts and ligand binding stabilize the aptamer by an additional ~6 ± 2 kcal/mol, in reasonable agreement with earlier measurements of the binding energy of 2-aminopurine (2AP), an adenine analog (*12*).

The distribution of forces, $p(F)$, for unfolding the fully folded aptamer (Fig. 2B) is well fit by an expression derived by Dudko *et al.* (*20*) for unfolding at fixed loading rate, parameterized by k_{off}, the unfolding rate at $F = 0$; $\Delta x^{\ddagger}$, the distance to the transition state from the folded state; and $\Delta G^{\ddagger}$, the height of the energy barrier (*18*). More than 3000 FECs measured for eight molecules, at loading rates varying from ~10 to 200 pN/s, yielded an unfolding rate $k_{off} \sim 0.04\ s^{-1}$ ($\ln k_{off} = -3.5 \pm 1$), similar to the value of $0.15\ s^{-1}$ measured previously by bulk kinetic methods (*12*). The activation

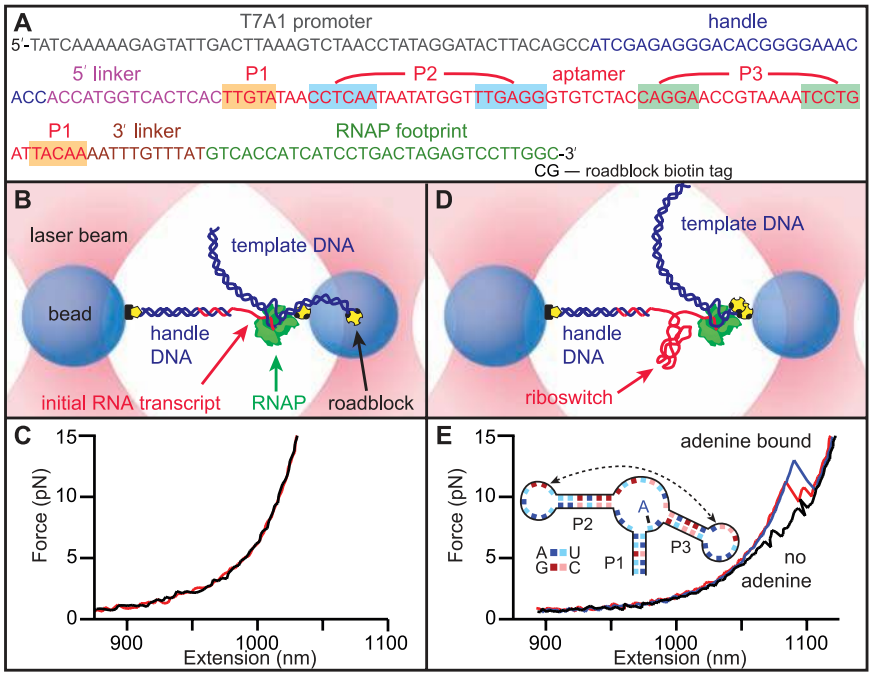

Fig. 1. (**A**) DNA template used for RNA transcription, showing the sequence of the nontranscribed promoter, the 25-bp section hybridizing with the DNA handle, the *pbuE* riboswitch aptamer (base-paired helices highlighted) flanked by short linkers, and the footprint of RNAP when stalled by the terminal roadblock. (**B**) Schematic of the optical trapping assay showing experimental geometry, with stalled RNAP and initial RNA transcript hybridized to the dsDNA handle (not to scale). (**C**) Two FECs obtained before aptamer transcription show little or no structure in the initial transcript. (**D**) Template DNA is transcribed in situ, producing an aptamer transcript, after which RNAP is stalled by a streptavidin molecule bound to the biotin-based roadblock. (**E**) FECs obtained after transcription show unfolding transitions in the aptamer. Without adenine, two events are seen (black), corresponding to the unfolding of hairpins P2 and P3 (inset). With adenine bound to the aptamer, larger unfolding events are observed (blue), sometimes involving an intermediate state (red).

[1]Department of Applied Physics, Stanford University, Stanford, CA 94305, USA. [2]Biophysics Program, Stanford University, Stanford, CA 94305, USA. [3]Department of Biological Sciences, Stanford University, Stanford, CA 94305, USA. [4]Department of Physics, University of Alberta, Edmonton AB, T6G 2G7, Canada. [5]National Institute for Nanotechnology, National Research Council of Canada, Edmonton AB, T6G 2M9, Canada.

*These authors contributed equally to this work.
†To whom correspondence should be addressed. E-mail: sblock@stanford.edu (S.M.B); michael.woodside@nrc.ca (M.T.W.)

Downloaded from www.sciencemag.org on March 19, 2008

energy, $\Delta G^{\ddagger}$, was 17 ± 4 kcal/mol, in agreement with a previous result for the unbinding of 2AP (*12*). The distance to the transition state $\Delta x^{\ddagger}$ was 2.1 ± 0.2 nm. Given an extension of ~0.42 nm/nt at the average unfolding force of ~15 pN, this result indicates that the transition state involves the unzipping of ~2.5 base pairs (bp) in helix P1, suggesting that the G:C base pair in P1 (Fig. 1E, inset) represents a structural keystone: Both the binding pocket and triple-helix junction unfold once it is disrupted. Isolated G:C base pairs located 3 to 4 bp from the loop of P1 are found in the other purine riboswitches, suggesting that they may be an important structural feature of this class of aptamers.

The kinetics of refolding and ligand binding were probed by observing the fraction of FECs showing the unfolding signature of the fully folded, adenine-bound aptamer, as a function of adenine concentration and the variable time interval during which refolding could occur between successive measurements (Fig. 3). We fit these data to a minimal, two-step model (Fig. 3, inset): formation of an intermediate structure competent to bind adenine (taken to be effectively irreversible) followed by adenine binding. The complete folding process involves a hierarchy of several steps, including folding of the three helices, formation of the loop-loop contacts and the adenine binding pocket, and binding of adenine. At $F = 0$, however, helix formation should be fast compared to formation of the tertiary

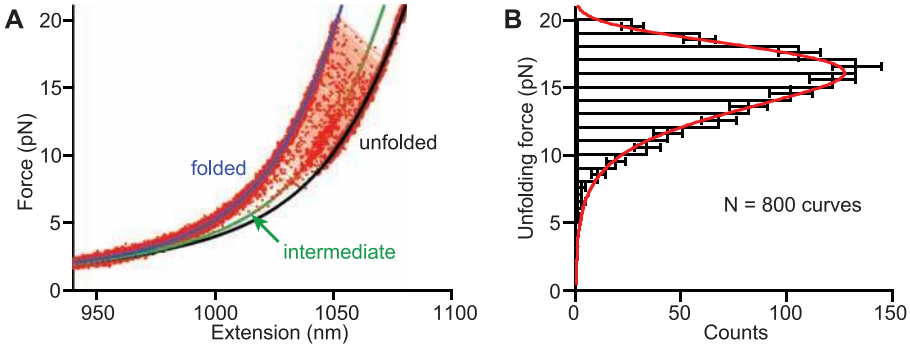

Fig. 2. (**A**) Nonequilibrium FECs for folded aptamer display a wide distribution of unfolding forces. WLC fit to the folded state (blue), and double WLC fits to the intermediate (green) and unfolded (black) states, indicate contour length changes of 39 ± 1 nt and 62 ± 1 nt for unfolding to the intermediate and unfolded states, respectively. (**B**) The unfolding force distribution is fit by a model returning the unfolding rate, along with the location and height of the energy barrier to unfolding.

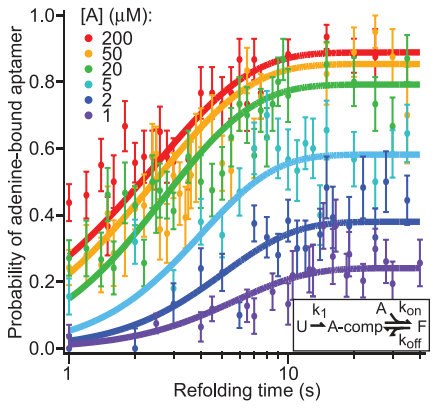

Fig. 3. Kinetics of aptamer refolding and binding. The fraction of FECs corresponding to the fully folded, adenine-bound aptamer (identified by the appropriate unfolding signature) for various adenine concentrations as a function of the variable time delay for refolding between pulls. Solid curves display the global fit to a minimal three-state kinetic scheme (**inset**): U, unfolded; A-comp, competent to bind adenine; F, folded (adenine-bound aptamer).

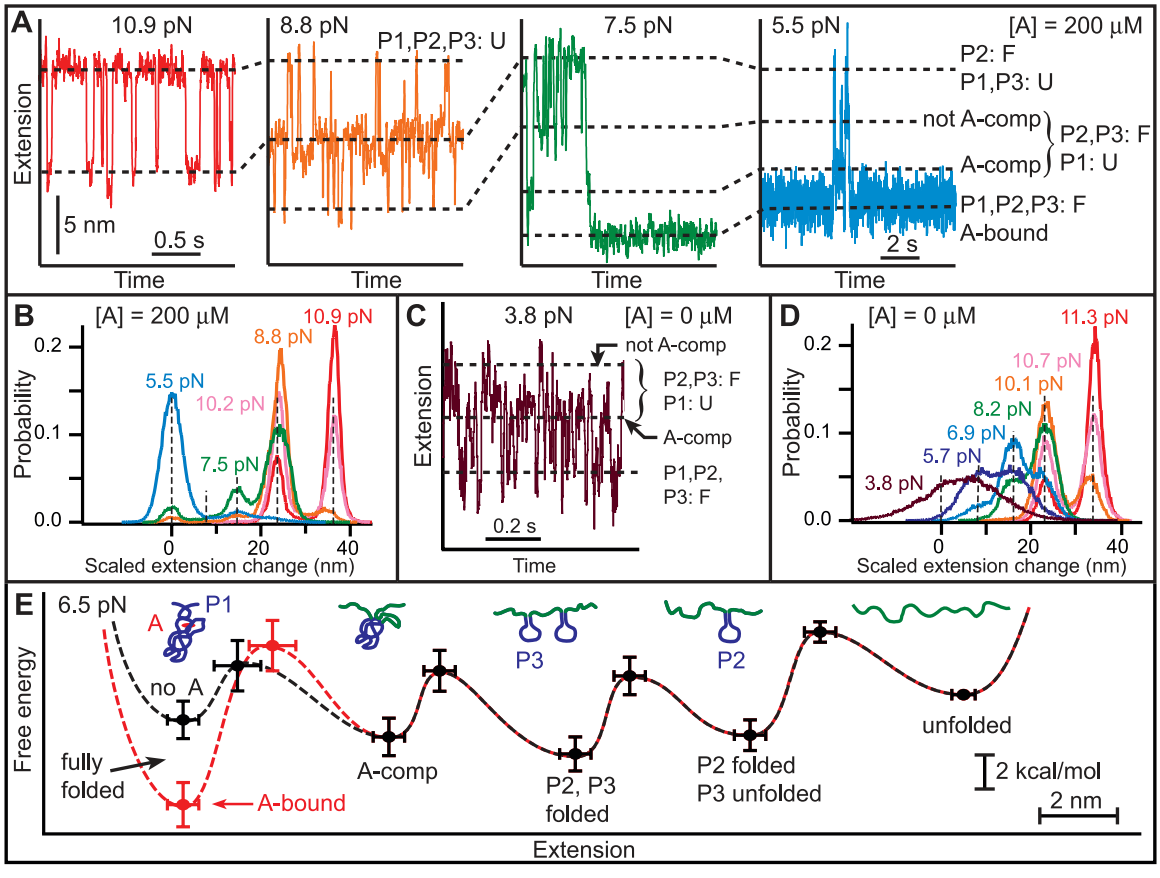

Fig. 4. Aptamer states and energetics determined by refolding at constant force. (**A**) As force is reduced, first P2 refolds (red), then P3 folds (orange). At lower forces, P2 and P3 interact to form a binding pocket and adenine binds, generating two additional states (green). The adenine-bound state is stable over many seconds, even at 5 pN load (blue). (**B**) Histograms of complete trajectories at different forces, with extension changes scaled by the force-dependent extension per nucleotide. Dashed lines indicate distinct states; the A-comp state is rarely populated. (**C** and **D**) Refolding trajectory and histograms in the absence of adenine. P2 and P3 folding occur as with adenine, but the A-comp state is highly populated at low force, whereas the folded state is very unstable, even at low force (purple). (**E**) Quantitative energy landscapes for aptamer folding at 6.5 pN, reconstructed from the experimental data in the presence (red) and absence (black) of adenine. The five potential wells correspond to five observed folding states, illustrated by cartoons. Adenine binding only appreciably affects the barrier and energy of the folded state.

Downloaded from www.sciencemag.org on March 19, 2008

interactions creating the binding pocket; hence, we model this process using just three distinct states. A global fit of data to the time-dependent folding probabilities returned $k_1 = 0.4 \pm 0.05\ s^{-1}$, $k_{off} = 0.2 \pm 0.05\ s^{-1}$, and $k_{on} = 8 \pm 1 \times 10^4\ M^{-1}\ s^{-1}$. The value of k_{off} is similar to that obtained above, and k_{on} is close to the value measured by bulk experiments (*12*). The slow folding rate implies that both aptamer folding and adenine binding occur on the same time scale as transcription itself, supporting the hypothesis that the function of this riboswitch is governed by folding and binding kinetics rather than equilibrium thermodynamics (*10*, *26*).

The multiple steps in the overall folding reaction were studied in greater detail by unfolding the aptamer completely and monitoring its extension under constant force with a passive force clamp (*27*) as the force was reduced stepwise every 1 to 2 min. Observing the transitions in the refolding process individually, based on their different energies and time scales, four distinct steps were seen (Fig. 4). The first folding event, at ~9 to 11 pN (Fig. 4A, red), involves length changes and force-dependent kinetics consistent with folding the 21-nt hairpin P2, as predicted by an energy landscape model for hairpin folding (*16*, *18*). The second folding step, at ~7 to 8 pN (Fig. 4A, orange), matches the properties expected for folding the 19-nt hairpin P3. The identification of these steps with the folding of P2 and P3 was confirmed by blocking the folding of each hairpin separately with antisense oligomers (fig. S3). We speculate that P2, the first fully transcribed element, is also the most stable in order to ensure that it can form in the presence of competing, alternative secondary structures in the upstream mRNA that might delay or prevent the formation of the proper aptamer structure.

In contrast to the adenine-independent events described above, the two folding transitions observed at lower forces were found to be adenine-dependent. For forces below ~7 pN at saturating adenine concentrations, the aptamer spent considerable time in the shortest-extension state (Fig. 4A, green and blue), which we identify as the folded, adenine-bound state. That identification was confirmed by measuring a contour length change of 63 ± 1 nt when the 63-nt aptamer was completely unfolded from this state. The contour length change between this state and the one with only P2 and P3 folded, 21 ± 2 nt, is consistent with the 23 nt that are not involved in P2 and P3 folding. In addition, a transient intermediate was observed between these two states, 14 ± 1 nt from the folded state. Because there are 15 nt in and adjacent to P1 (Fig. 1A), we identify this intermediate as a state where P2 and P3 are folded and the adenine binding pocket is preorganized by tertiary contacts, sequestering the nucleotides between P2 and P3, but P1 remains unfolded. The extensions of all five states (fully unfolded, P2 folded, P2/P3 folded, P1 unfolded, and fully folded), scaled by the fractional extension per nucleotide at a given force, are evident in histograms of records (Fig. 4B).

Constant-force–extension records in the absence of adenine (Fig. 4, C and D) indicate very different behavior at low forces: The P1-unfolded state is strongly populated below ~6 pN, whereas the folded state is only well populated below ~4 pN. Even at such low forces, the folded-state lifetime is short, with a rapid equilibrium between folded and P1-unfolded states. These differences can be understood if the P1-unfolded state is the adenine-competent state. At saturating adenine concentrations, the formation of this state leads rapidly to an adenine-bound, folded state that is long-lived even at ~7 pN (Fig. 4A), and the P1-unfolded state is thus rarely occupied. In contrast, absent adenine, the P1-unfolded state is frequently occupied even at low forces. Occasionally, the transient folding of P1 was observed even with adenine present (Fig. 4A, green), likely indicating that adenine was not bound at that instant. The single-molecule records thus directly reflect an adenine-induced stabilization of helix P1 that underpins the switching action of the riboswitch (*28*).

Each of the folding transitions can be analyzed individually as a two-state process, enabling a piecewise reconstruction of the energy landscape for folding, both with and without adenine (Fig. 4E). The relative free energies of the five observed states were determined from extension histograms, and the locations and heights of the energy barriers between states were determined from the force dependence of the kinetics (*15*, *18*). From these landscapes, we find that the tertiary contacts that form the adenine-competent state, which are primarily base-pair and base-quartet interactions between the hairpin loops (*4*, *9*), stabilize the structure by an additional 2.7 ± 0.3 kcal/mol (*18*). The transition state for breaking these interactions lies ~1 nm from the adenine-competent state, indicative of their short range (*29*). We also find that adenine binding stabilizes the folded state by 4 ± 1 kcal/mol and raises the energy barrier for leaving the folded state, but does not appreciably affect other properties of the landscape.

These energy landscapes dramatically illustrate the sequential folding of each structural element in the RNA. Folding proceeds through a distinct hierarchy of states, but the formation of tertiary and secondary structure is interleaved, because the energetic stabilities of these structures happen to be comparable, in contrast with the standard picture of hierarchical folding. Indeed, the tertiary contacts that preorganize the adenine-competent state are considerably more stable than the least-stable helix, P1, which is the essential component governing the switching behavior of the riboswitch. In vivo, without adenine binding to stabilize P1, this last component of the aptamer to fold would be highly susceptible to disruption by terminator hairpin invasion.

The techniques developed here point the way to a powerful method for monitoring cotranscriptional folding. In the case of the *pbuE* aptamer, the first FEC obtained after transcription did not exhibit an unfolding behavior substantially different from that of subsequent FECs, implying that the cotranscriptional aspect of folding may not be important for the formation of an isolated aptamer (*18*). This result is unsurprising, because structural elements of the aptamer fold in the same order as they are transcribed; hence, force-induced refolding mimics cotranscriptional folding in this case. However, for the folding of the complete riboswitch, which includes a downstream terminator hairpin that competes with aptamer formation, we anticipate an important cotranscriptional dependence (*10*, *26*).

References and Notes

1. W. C. Winkler, R. R. Breaker, *Annu. Rev. Microbiol.* **59**, 487 (2005).
2. R. L. Coppins, K. B. Hall, E. A. Groisman, *Curr. Opin. Microbiol.* **10**, 176 (2007).
3. R. T. Batey, S. D. Gilbert, R. K. Montange, *Nature* **432**, 411 (2004).
4. A. Serganov *et al.*, *Chem. Biol.* **11**, 1729 (2004).
5. M. Mandal *et al.*, *Cell* **113**, 577 (2003).
6. J. Noeske *et al.*, *Proc. Natl. Acad. Sci. U.S.A.* **102**, 1372 (2005).
7. S. D. Gilbert, C. D. Stoddard, S. J. Wise, R. T. Batey, *J. Mol. Biol.* **359**, 754 (2006).
8. J. Noeske *et al.*, *Nucleic Acids Res.* **35**, 572 (2007).
9. O. M. Ottink *et al.*, *RNA* **13**, 2202 (2007).
10. J. F. Lemay *et al.*, *Chem. Biol.* **13**, 857 (2006).
11. M. Mandal, R. R. Breaker, *Nat. Struct. Mol. Biol.* **11**, 29 (2004).
12. J. K. Wickiser, M. T. Cheah, R. R. Breaker, D. M. Crothers, *Biochemistry* **44**, 13404 (2005).
13. E. A. Abbondanzieri, W. J. Greenleaf, J. W. Shaevitz, R. Landick, S. M. Block, *Nature* **438**, 460 (2005).
14. I. Tinoco Jr., C. Bustamante, *Biophys. Chem.* **101-102**, 513 (2002).
15. M. T. Woodside *et al.*, *Science* **314**, 1001 (2006).
16. M. T. Woodside *et al.*, *Proc. Natl. Acad. Sci. U.S.A.* **103**, 6190 (2006).
17. R. V. Dalal *et al.*, *Mol. Cell* **23**, 231 (2006).
18. Materials and methods are available as supporting material on *Science* Online.
19. B. Onoa *et al.*, *Science* **299**, 1892 (2003).
20. O. K. Dudko, G. Hummer, A. Szabo, *Phys. Rev. Lett.* **96**, 108101 (2006).
21. S. B. Smith, Y. Cui, C. Bustamante, *Science* **271**, 795 (1996).
22. Y. Seol, G. M. Skinner, K. Visscher, *Phys. Rev. Lett.* **93**, 118102 (2004).
23. W. Saenger, *Principles of Nucleic Acid Structure* (Springer, New York, 1984).
24. J. Liphardt, S. Dumont, S. B. Smith, I. Tinoco Jr., C. Bustamante, *Science* **296**, 1832 (2002).
25. C. Jarzynski, *Phys. Rev. Lett.* **78**, 2690 (1997).
26. J. K. Wickiser, W. C. Winkler, R. R. Breaker, D. M. Crothers, *Mol. Cell* **18**, 49 (2005).
27. W. J. Greenleaf *et al.*, *Phys. Rev. Lett.* **95**, 208102 (2005).
28. Some molecular heterogeneity was present, but we did not observe order-of-magnitude variations in the kinetics from one RNA to the next, as reported in one single-molecule fluorescence study (*10*).
29. P. T. X. Li, C. Bustamante, I. Tinoco Jr., *Proc. Natl. Acad. Sci. U.S.A.* **103**, 15847 (2006).

30. We thank R. Landick for providing purified RNAP, K. Herbert for providing the plasmid used to make the transcription template, M. Larson and O. Dudko for helpful advice, and members of the Block lab and Program Project grant GM066275 for useful discussions. Our research was supported by grants from the National Institute of General Medical Sciences (GM057035) and the National Institute for Nanotechnology.

Supporting Online Material

www.sciencemag.org/cgi/content/full/1151298/DC1
Materials and Methods
Figs. S1 to S3
Tables S1 and S2
References

3 October 2007; accepted 11 December 2007
Published online 3 January 2008;
10.1126/science.1151298
Include this information when citing this paper.

Downloaded from www.sciencemag.org on March 19, 2008

www.sciencemag.org/cgi/content/full/1151298/DC1

Supporting Online Material for

Direct Observation of Hierarchical Folding in Single Riboswitch Aptamers

William J. Greenleaf, Kirsten L. Frieda, Daniel A. N. Foster, Michael T. Woodside,* Steven M. Block*

*To whom correspondence should be addressed. E-mail: sblock@stanford.edu (S.M.B); michael.woodside@nrc.ca (M.T.W.)

Published 3 January 2008 on *Science* Express
DOI: 10.1126/science.1151298

This PDF file includes:

Supporting Online Material

Materials and Methods

Constructs. A 78 bp DNA fragment coding for the *pbuE* riboswitch aptamer was inserted into a pALB3 plasmid 31 bp downstream from a T7A1 promoter (Fig. 1A). An extra 9 bp were included in the insert at the 5′ end of the aptamer sequence, so that ~40 nt of ssRNA would be transcribed prior to the aptamer-containing region. The first 25 nt of the transcript were designed to hybridize with the 5′ cohesive end of a dsDNA handle, leaving a ~15-nt RNA linker region between the DNA handle and the aptamer structure after transcription. The 770-bp dsDNA transcription template was amplified by PCR from the cloned plasmid such that the template ended with a terminal biotin label 41 bp downstream of the aptamer sequence. The PCR product was incubated in a ~20-fold excess of streptavidin (ProZyme) at room temperature for 5 min to bind the streptavidin to the downstream terminus of the DNA template, followed by a ~1000-fold excess of biotin to saturate any unused streptavidin binding sites, and then purified. The final product was a DNA template coding for the *pbuE* riboswitch aptamer carrying a terminal streptavidin roadblock downstream. Because the RNAP molecule has a ~30 bp footprint on the DNA template (*S1*), the aptamer part of the transcript is anticipated to be separated from the polymerase by ~11 nt of RNA once transcription is stopped by the roadblock. This allows the aptamer to be unfolded and refolded without being perturbed by the nearby RNAP enzyme.

Biotinylated RNAP molecules were initiated on the T7A1 promoter of the transcription template. By omitting UTP from the initiation reaction, these became stalled at the first T residue of the template, after first transcribing 29 nt of RNA, as previously described (*S2*). The stalled transcription elongation complexes (TECs) were purified of free NTPs using a size-exclusion column. A 3057 bp-long dsDNA handle with a 5′ overhang of 25 nt ssDNA complementary to the first 25 nt of the RNA transcript was created as previously described (*S3*) by autosticky PCR of the M13mp18 plasmid, and then incubated with a near-stoichiometric amount of the stalled TEC at room temperature for 1 hr. The resulting mixture was incubated for 1 hr at room temperature with near-stoichiometric amounts of 600-nm diameter, avidin-coated polystyrene beads and 730-nm diameter, antidigoxigenin-coated polystyrene beads at an overall concentration of each of the components of ~1 nM. This final incubation was diluted ~20-fold into an RNase-free oxygen-scavenging buffer system consisting of 40 U/mL glucose oxidase (Calbiochem), 185 U/mL catalase (Sigma), and 8.3 mg/mL glucose (Sigma) in transcription buffer (50 mM HEPES pH 8.0, 130 mM KCl, 4 mM $MgCl_2$, 0.1 mM EDTA, 0.1 mM DTT), and placed in a flow chamber on a microscope slide. Transcription was initiated *in situ* by introducing a buffer containing 1 mM NTPs into the flow chamber.

Optical trap. The optical trapping apparatus used in these measurements has been described previously (*S4*). Briefly, a laser beam (1064 nm; Spectra-Physics) was split into two separately controlled traps by polarization, with one trap much stiffer than the other. The strong trap was steered in the specimen plane by acousto-optic deflectors (AODs; IntraAction Inc.), while the position of the bead held in the weak trap was monitored by collecting the light from a second laser (830 nm; Point Source) scattered off the bead onto a position sensitive detector (Pacific Silicon Sensors). Force-extension curves (FECs) were measured by moving the traps apart at a constant velocity using the AODs. Discrete data points in the FECs represented 2.5 ms of signal integration time, acquired using custom Labview software (National Instruments). Refolding at constant force was measured using the passive force clamp technique described previously (*S5*),

in order to avoid spurious instrumental artefacts arising from active feedback loops (*S6*). Some refolding records were also measured in an "open-loop" configuration, without a force clamp. Data in refolding records were sampled at 4 kHz and filtered at 2 kHz with an 8-pole Bessel filter (Krohn-Hite). All measurements in the optical trap were taken at a sample temperature of ~24°C. The temperature of the room was controlled to within ±0.2°C.

Force-extension curves. The presence of single DNA tethers held in the dumbbell arrangement (Fig. 1B) was confirmed by measuring the contour lengths and persistence lengths of the DNA handle from FECs obtained at low forces (dumbbells found to be connected by multiple tethers were excluded from further analysis). FECs without adenine present were measured after transcription without any change of buffer. FECs with adenine present were measured after washing the flow chamber with at least 3 volumes of transcription buffer containing the desired adenine concentration. For measurement of low concentrations of adenine (<20 μM), transcription buffer with 20 μM adenine was flushed into the flow cell and incubated for 10 min. Then, the buffer was replaced with a buffer containing the final adenine concentration desired, followed by ~5 min of incubation and at least one more wash with the low adenine concentration buffer. These wash steps ensured that any propensity of adenine to stick to the flow chamber surfaces would not reduce the overall concentration of free adenine in solution. Where not otherwise indicated in the text, FECs were measured with a constant delay time before each pull of 3 s, in the presence of 200 μM adenine.

FECs were partitioned into folded, intermediate, and unfolded states based on the structure of the sawtooth unfolding pattern, as seen in Fig. 1E. The results of multiple measurements were aligned to remove the small amount of residual instrumental drift (~2 nm or less) that occurred over the course of the experiment, then averaged. The average FEC for the folded state was fit to a single worm-like chain (WLC) model using a modified Marko-Siggia interpolation formula (*S7*):

$$F(x) = \frac{k_B T}{L_p}\left[\frac{1}{4}\left(1 - \frac{x}{L_c} + \frac{F}{K}\right)^{-2} - \frac{1}{4} + \frac{x}{L_c} - \frac{F}{K}\right], \quad (1)$$

where L_c is the contour length of the handle, L_p is the persistence length, K is the elastic modulus, and k_B is Boltzmann's constant. The average FECs for the intermediate and unfolded states were then fit to a double WLC model, which included terms for both the extension of the dsDNA handle (as determined by the fit to the folded-state FEC) and for the extension of the now-unfolded ssRNA. Previous work (*S8*-*S13*) has reported a range of values for the persistence length of ssRNA, which has been found to be sequence-dependent (*S9*); an average value of 1.0 nm was used for the fits performed here. The ssRNA elastic modulus was taken to be 1600 pN/nm (*S8*), and a ssRNA contour length of 0.59 nm/nt, a value expected from the structure of the 3′ endo sugar pucker, was assumed (*S14*). The width of the A-form helix was taken to be 2.2 nm (*S14*); this width was subtracted from the extension of the folded state when fitting the FECs to determine the number of nucleotides released during complete unfolding.

We note that the observed contour length change (corresponding to 62 ± 1 nt) indicates that the adenine-bound, folded state likely does not exhibit any significant "fraying" of helix P1 under tension, despite the fact that the two closing basepairs of P1 are comparatively weak AU pairs. This result contrasts with the fraying previously observed in DNA hairpins with different weak

closing sequences (*S15*, *S16*), suggesting that tertiary interactions with the nearby binding pocket may supply additional mechanical stability.

FECs with a structure that indicates that adenine did not bind to the aptamer are displayed in Fig. S1. Three states can be observed. As seen previously when adenine does bind (Fig. 2A), one portion of the FEC corresponds to a well-defined unfolded state (63 ± 2 nt of ssRNA), and another corresponds to an intermediate state whose contour length is 22 ± 2 nt shorter. At low force, however, the adenine-free FEC is fit by a WLC with 24 ± 2 nt of ssRNA still present. Thus, the three states involve ~39 nt folded, ~22 nt folded, and 0 nt folded, implying that just prior to the first unfolding event in these FECs, only P2 and P3 are folded (40 nt in total), after which P3 unfolds, leaving only P2 folded (21 nt), before P2 finally unfolds.

Force distributions. Unfolding force distributions created by measuring the first unfolding event from the fully-folded state in each FEC were fit to the non-equilibrium model of Dudko *et al* (*S17*):

$$p(F) \propto \frac{k(F)}{r} \exp\left\{ \frac{k_{\text{off}}}{\Delta x^{\ddagger} r} - \frac{k(F)}{\Delta x^{\ddagger} r}\left(1 - \frac{\Delta x^{\ddagger} F}{\Delta G^{\ddagger}} \nu \right)^{1-1/\nu} \right\}, \tag{1}$$

$$\text{where } k(F) = k_{\text{off}} \left(1 - \frac{\Delta x^{\ddagger} F}{\Delta G^{\ddagger}} \nu \right)^{1/\nu - 1} \exp\left\{ \Delta G^{\ddagger} \left[1 - \left(1 - \frac{\Delta x^{\ddagger} F}{\Delta G^{\ddagger}} \nu \right)^{1/\nu} \right] \right\},$$

k_{off} is the unfolding rate at 0 force, $\Delta x^{\ddagger}$ is the distance to the transition state from the folded state, $\Delta G^{\ddagger}$ is the height of the energy barrier, and ν is a parameter characterizing the shape of the energy barrier (ν = 1/2 for a sharp, cusp-like barrier; ν = 2/3 for a softer, cubic potential). The shape of the barrier is unknown, but the cusp-like and cubic models represent two reasonable limiting cases. For all fitting parameters, the two models gave results that were equal within uncertainty: Assuming a sharp, cusp-like barrier, we obtained an average unfolding rate for all molecules measured of $k_{\text{off}} \sim 0.03\ \text{s}^{-1}$, an average distance to the barrier of $\Delta x^{\ddagger} = 2.1 \pm 0.2$ nm, and an average barrier height of $\Delta G^{\ddagger} = 19 \pm 4$ kcal/mol. Assuming instead a softer, linear-cubic potential landscape, the average results were $k_{\text{off}} \sim 0.04\ \text{s}^{-1}$, $\Delta x^{\ddagger} = 2.1 \pm 0.2$ nm, and $\Delta G^{\ddagger} = 15 \pm 4$ kcal/mol. Thus the principal difference between these alternative models would seem to be in the height of the barrier returned, and even that quantity is found to be the same within our experimental uncertainty. We therefore averaged the results obtained with both these models to obtain the rates and energetics derived from our data reported here. The rate k_{off} is highly sensitive to the force, hence the uncertainty in k_{off} is expressed in terms of $\ln(k_{\text{off}})$ in the text.

Equilibrium free energy. The equilibrium folding free energy was calculated from the non-equilibrium FEC measurements using the method of Jarzynski (*S18*), which involves an exponentially-weighted mean of the irreversible work done to unfold the molecule. In order to calculate the irreversible work from the measured FEC, the energy required to stretch the molecular handles must also be taken into account, because this energy is not associated with the aptamer structure itself. Therefore, calculation of the relevant irreversible work involves first finding the work performed to stretch out the entire construct (including handles) and the work to unfold the aptamer, by integrating the measured FEC out to a point corresponding to the end of the last unfolding event, including any intermediates (Fig. S2, red shading). Then, the energy required to stretch out the handles and ssRNA to the identical force must be subtracted from this

work. The latter energy is calculated by integrating the FEC expected for the fully-unfolded state out to the same point (Fig. S2, black shading). This procedure is equivalent to integrating the FECs between constant extension endpoints (*e.g.*, 0 and some extension value above all unzipping events for a given molecule), calculating the weighted average, and subtracting the work done to stretch the handles, under the assumption that the handles are at equilibrium throughout the experiment. To reduce fluctuations from noise in the experimental FECs, these integrals were calculated from the unfolding forces measured in each FEC using the fits for the averaged FECs for folded, intermediate, and unfolded states (as shown in Fig. 2A).

The Jarzynski estimator is known to have a systematic bias when only finite numbers of measurements are sampled, due to nonlinear weighting of the data. We estimate the bias, under the assumption of a Gaussian free energy distribution (*S19*), as 3 ± 1 kcal/mol. This bias is included in the equilibrium free energy reported in the main text.

Kinetics from FECs. To measure refolding and binding kinetics, the aptamer was first completely denatured by exerting a large load (~20 pN). The load was then immediately reduced to ~0 pN by reducing the bead separation to ~350 nm (transition time <5 ms), a distance much less than the contour length of the 3-kb DNA handle. After a variable delay time to allow refolding to occur, a FEC was measured by immediately jumping the tension to ~2 pN and then moving the two traps apart at a rate of ~300 nm/s, until the force reached ~20 pN and the aptamer was once again denatured. FEC measurements were repeated 10-20 times for each desired value of the delay time, for at least two different molecules, and the fraction of FECs that had refolded to the fully-folded, adenine-bound structure was determined from the unfolding signature, as in Fig. 1.

The rates plotted in Fig. 3, with standard binomial error estimates, were fit to the time-dependent probability for the folded state as calculated from the rate equations corresponding to the 3-state reaction pathway (Fig. 3, inset). Because our constant-force measurements imply that the equilibrium free energy difference between fully-folded and adenine-competent states is ~6 k_BT, (Table S1), the folding of the adenine-competent state was taken to be effectively irreversible. We note that the experimental value for the refolding/binding saturated at ~90% at high adenine concentrations (rather than 100%), possibly due to some misidentification of a minor fraction of FECs, or to the presence of a long-lived unfolded or misfolded state. This saturation level was included when calculating rates for the three-state model.

From the measured binding and dissociation rates of adenine, the dissociation constant is $K_d = 2.5 \pm 0.7$ μM, implying a standard Gibbs free energy of 7.6 ± 0.2 kcal/mol at 24°C. This value is comparable to a previous result reported for the standard Gibbs free energy for 2AP binding (*S20*), ~8.3 kcal/mol (uncertainty not reported).

Hairpin unfolding predictions. A number of predictive models have been developed to describe the folding of hairpins under tension (*S16*, *S21*-*S23*). Here, we use an energy landscape model developed previously by our groups that has been extensively tested for DNA hairpin folding/refolding in an optical trap (*S15*, *S16*). We assume a ssRNA contour length of 0.59 nm/nt, and nearest-neighbor stacking energies that are 25% lower than the canonical values measured in 1 M salt, to account for the reduced salt concentration used in our assay buffer (*S24*). The results of the model are listed in Table S2 for hairpins P2 and P3. For comparison, the unfolding force, unfolding distance, and distance to transition state observed for the folding events correlated to P2 and P3 folding are listed in Table S1. To convert measured rates into

barrier heights, we assumed that the rates vary as $k = k_0\exp(-\Delta G^{\ddagger}/k_B T)$, where the prefactor k_0 was taken to be 10^5 s^{-1}, in accordance with previous measurements of the kinetics of unfolding DNA hairpins in an optical trap (*S16*). We estimated the uncertainties in the model predictions from the standard deviation of the results calculated using a range of ssRNA persistence lengths compatible with previous measurements (0.8-1.3 nm). Uncertainties in the stacking interactions and salt correction (assumed to introduce ~7% error) were added in quadrature.

We note that there is good overall agreement between the experimental observations and model predictions, with the exception of the opening force (hence also the folding free energy) for hairpin P2: the measured value is ~1-2 kcal/mol larger than predicted. Given the prior success of the model in predicting the behavior of hairpins for a wide range of stem sequences, we postulate that this discrepancy may be due to some extra stability in the loop of hairpin P2 imparted by intraloop base stacking and/or hydrogen bonding, or from the formation of additional, non-canonical base pairs in the stem of this hairpin, neither of which is considered by the model.

Refolding trajectories. Refolding trajectories were measured both in the presence and absence of 200 μM adenine. Data were filtered offline using a median filter with a 10 ms window, then partitioned into two or more states using a threshold algorithm similar to that previously described (*S16*). The extension change for each transition, Δx, was measured directly from Gaussian fits to position histograms formed from the extension records (*S15*, *S16*). The number of RNA nucleotides involved in each folding step was calculated from the extension change at a given force by adding (or subtracting, as appropriate) the width of an A-form helix, 2.2 nm, and dividing by the extension expected per nucleotide at that force, assuming a WLC model for ssRNA, as described above. For folding the P2 and P3 helices, one helix width was added to the observed extension change. For folding to the adenine-competent state, one helix was subtracted, because published structures of the purine riboswitches suggest that the loop-loop interaction that causes binding-pocket pre-organization arranges the 5′ end of P2 and the 3′ end of P3 approximately one helix-width away from each other (*S25*, *S26*). For folding P1, no helix correction was applied. The extension change upon fully unfolding the aptamer at the start of the refolding measurements, in the presence of adenine, was found to be 63 ± 1 nt, fully consistent with the FEC measurements.

Each folding transition was analyzed as a separate two-state system, as described previously (*S16*). Briefly, $F_{1/2}$, defined as the force at which a structural element spent equal time in folded and unfolded states, was determined by plotting the fraction of time spent unfolded as a function of force, and fitting this to the Boltzmann relation for a two-state system: $P_u(F) = \{1 + \exp[(F_{1/2} - F)\cdot\Delta x/k_B T]\}^{-1}$ (*S24*). The free energy for each folding step was then computed from the quantity $F_{1/2}\cdot\Delta x$, minus the energy required to stretch out the unfolded ssRNA (calculated from an integral of a worm-like chain of appropriate length). The average rate for transitions from state A to state B was calculated by dividing the number of transitions from A to B by the total amount of time spent in state A. The distance along the reaction coordinate to the transition state, $\Delta x^{\ddagger}$, was determined for each folding step from the force dependence of the rates. Assuming a sharp energy barrier, $\Delta x^{\ddagger}$ is given by the slope of the logarithm of the rates as a function of force, since $k(F) = k_0\exp(F\Delta x^{\ddagger}/k_B T)$ (*S27*). The results for each transition are summarized in Table S1. Extracting the rates for the final transition to the fully-folded, adenine bound state presented a special challenge, because adenine-binding shifts $F_{1/2}$ for this state to a value higher than $F_{1/2}$ for folding P3. Since P3 folding is required to form the adenine binding

pocket, the $F_{1/2}$ value for the adenine-bound folded state had to be extrapolated from data collected well below $F_{1/2}$, resulting in a comparatively large uncertainty.

The proper identification of the two folding events observed at the highest forces, corresponding to P2 and P3 folding, was confirmed by blocking the folding of each of these hairpins separately, using anti-sense oligomers complementary to the loop and 3′ stem of hairpin P2 (denoted "anti-P2") or the loop and 5′ stem of hairpin P3 (denoted "anti-P3"). Comparing folding trajectories measured at ~11 pN with and without the anti-P2 oligomer, the bistable behavior attributed to folding and unfolding of hairpin P2 (Fig. S3A, red) is suppressed by the presence of the anti-P2 oligomer (Fig. S3A, blue), confirming the identification. Similarly, the transition at ~8 pN attributed to hairpin P3 is suppressed by the anti-P3 oligomer (Fig. S3B). Notably, however, the P2 folding transition is not affected by the anti-P3 oligomer, as seen in Fig. S3B (blue) from the upward spike, corresponding to P2 folding.

The conformation of the adenine-competent state was determined by comparing the length changes observed between this state and both P2/P3-folded and the fully folded states. The observed length change of 7 ± 1 nt between the P2/P3-folded and adenine-competent states implies that the stems of P2 and P3 are brought into contact in the adenine-competent state, so that J2-3 (the 8-nt junction segment between P2 and P3) is no longer stretched out. This contact is likely maintained by interactions between the loops of the hairpins and by base-paring between the terminal G and C residues of J2-3 (*S26*). On the other hand, the length change of 14 ± 1 nt between the adenine-competent and fully-folded states indicates that the 15 residues in P1, J1-2 (the junction segment between P1 and P2), and J3-1 (the junction segment between P3 and P1) are still unfolded in the adenine-competent state. Thus, in the adenine-competent state, the residues in P1, J1-2, and J3-1 are stretched away from the junction, and hence not available for creating tertiary contacts with J2-3. This forms the basis for our claim that the adenine-competent state is stabilized largely by contacts between the loops, rather than in the junction. This interpretation finds additional support in NMR structures of the guanine riboswitch aptamer (*S28*), in which structural changes upon ligand binding were seen to occur predominantly in the J2-3 and P1 regions, suggesting that most tertiary interactions in the junction are not present in the absence of ligand.

We do not observe evidence for an additional intermediate state between the P2/P3 folded and adenine-competent states, as postulated by Lemay *et al*. to explain their single-molecule FRET data (*S29*). This may be attributable to differences in the experimental conditions, including buffer conditions or the effects of tension on the RNA molecule.

Extension histograms obtained at different forces were compared (Figs. 4B, D) by first scaling the measured extension changes by the fractional extension of the ssRNA (*i.e*., the extension per nucleotide divided by the contour length per nucleotide) at a particular force, as given by the WLC model. This is not quite the same as the true contour length change, since corrections for the creation or dissolution of helices are not included.

Free energy landscapes. Free energy landscapes (Fig. 4E) are depicted at a constant force based on the relative free energies of the 5 different states determined in the refolding trajectories, and on the locations and heights of the energy barriers between the various states determined from the force-dependent kinetics. Rates under tension were converted into energy barriers assuming the prefactor $k_0 = 10^5\ s^{-1}$, as determined previously in an optical trapping study of DNA hairpins (*S16*). Due to experimental uncertainties, the sum of the distances to the transition state from

folded and unfolded states did not always precisely equal the total unfolding distance. In these cases, the distances to the transition state were scaled so that their sum was equal to the total distance. Note that these diagrams represent the effective potential landscape under tension, and hence include the stretching energy of the unfolded ssRNA.

Note that the transition state for leaving the adenine-bound, folded state, as measured from the refolding trajectories at constant force, involves unfolding the folded state by a distance corresponding to ~6 nt. This distance matches the result from the non-equilibrium unfolding measurements, reinforcing the conclusion that the barrier to P1 unfolding occurs near the G:C pair in helix P1.

Co-transciptional folding. The question of whether aptamer folding is different when occurring concurrently with transcription (co-transcriptional folding) was addressed by comparing the first FEC measured immediately after transcription of the aptamer to all the FECs measured subsequently, for each molecule. Such comparisons were made for 23 molecules. No differences in the unfolding distance, unfolding force, or fraction of events displaying unfolding intermediates were evident in our data, suggesting that folding of the aptamer is the same whether formed co-transcriptionally or by refolding after mechanical disruption.

Primary Sources of Experimental Error. The experimental uncertainties cited above and in the main text and figures include the effects of both statistical and systematic errors. The principal source of random error in these experiments is the variation in the sizes of beads, which leads directly to an uncertainty in position measurements (estimated at ~5–10%) and also, indirectly, to calibration errors in force associated with changes in the distribution of scattered light that lead to an uncertainty in the effective trap stiffness (estimated ~10%). Such errors are reduced by making measurements on as many beads as possible. An additional source of error in constant force measurements comes from uncertainty in the location of the zero-stiffness position in the optical trap (*S5*). We estimate that residual stiffness, associated with being displaced from the center of the zero-stiffness region of the trap, could introduce an uncertainty of up to 5-10% in distance measurements.

The principal source of systematic error arises from the calibration of trap stiffness. We estimate our systematic error in force to be ~10-15%. A second source of systematic error, relevant to the FEC analysis, comes from the fact that unfolding events at very low force (<5 pN) are typically difficult to observe, effectively truncating the force distribution. This may serve to increase the effective bias in the Jarzynski estimate of the equilibrium free energy (*S19*).

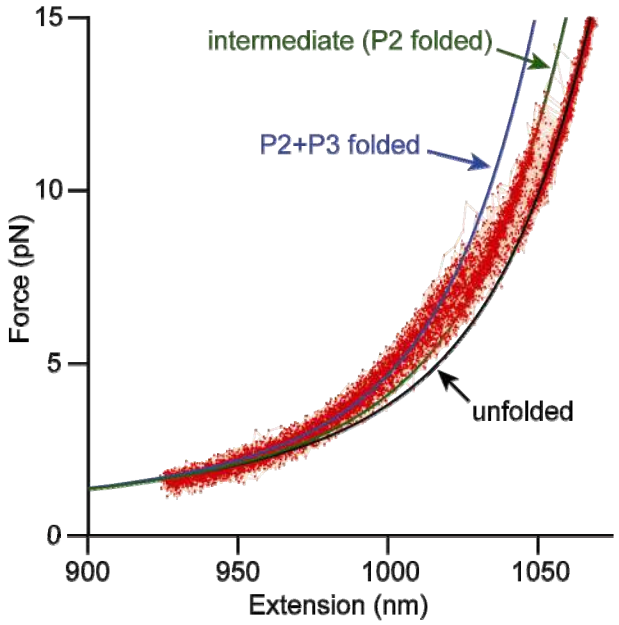

Fig. S1. FECs observed when adenine is not bound to the aptamer (same molecule as Fig. 2A). Two unfolding events are seen. The first event involves unfolding of P3; the second event involves the unfolding of P2, the same as the intermediate seen in Fig. 2A.

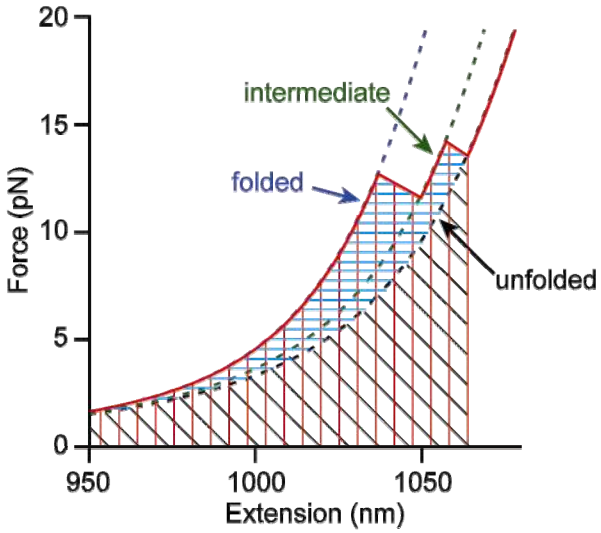

Fig. S2. Graphical representation of the work performed during stretching. The non-equilibrium work done to unfold the aptamer (blue) is given by the area under the measured FEC out to the last unfolding event (red), minus the area under the unfolded state FEC out to the same point (black).

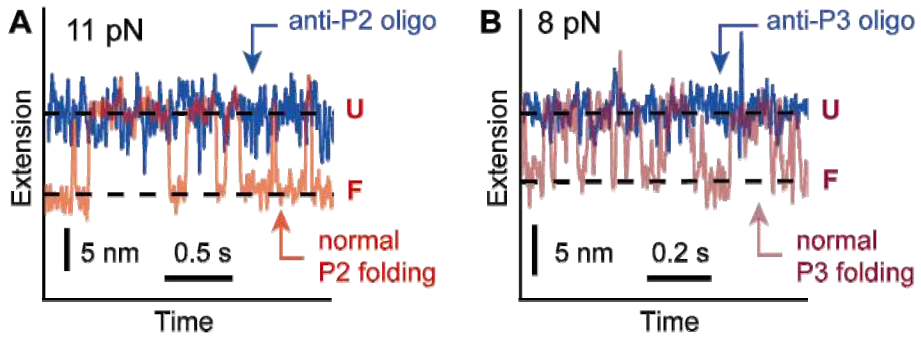

Fig. S3. Refolding traces in presence and absence of anti-sense oligos. (A) In the presence of an anti-P2 oligo, the normal folding of P2 at ~9-11 pN (red) is suppressed (blue). (B) In the presence of an anti-P3 oligo, the normal folding of P3 at ~7-8 pN (purple) is suppressed (blue). Note that the normal unfolding of P2, evident as a brief increase in extension (blue), is not suppressed by the presence of an anti-P3 oligo. Extensions of records obtained with and without oligos have been aligned on the common unfolded state to remove any drift occurring during buffer exchange.

Table S1. Measured values describing individual folding steps of *pbuE* aptamer. The four steps are: P2 folding, denoted "P2"; P3 folding, denoted "P3"; adenine-competent state folding, denoted "AC" (adenine-competent); and full folding with adenine bound, denoted "AF" (adenine; folded), or full folding in the absence of adenine, denoted "NAF" (no adenine; folded). Distances are reported in nm for forces as close as possible to $F_{1/2}$, except in the case of AF (for which $F_{1/2}$ could not be reached). Values were determined from measurements on 3 different molecules in the absence of adenine and 7 in the presence of adenine. Uncertainty estimates do not include systematic errors in force arising from trap stiffness calibration.

Folding step	**Δx (nm)**	**Δx (nt)**	**$F_{1/2}$ (pN)**	**$\ln k_{1/2}$ (s^{-1})**	**$\Delta G^{\ddagger}_{1/2}$ (kcal/mol)**	**$\Delta x_f^{\ddagger}$ (nm)**	**$\Delta x_u^{\ddagger}$ (nm)**
P2	6.4 ± 0.5	22 ± 1	10.0 ± 0.8	2.9 ± 0.3	5.2 ± 0.6	2.5 ± 0.4	5.1 ± 0.6
P3	4.6 ± 0.5	20 ± 1	7.0 ± 0.6	4.1 ± 0.3	4.4 ± 0.6	1.8 ± 0.3	4.1 ± 0.6
AC	4.1 ± 0.5	7 ± 1	5.1 ± 0.5	4.5 ± 0.6	4.2 ± 0.7	1.4 ± 0.4	3.7 ± 0.6
AF	4.2 ± 0.5	14 ± 1	9 ± 1	0 ± 1	7 ± 1	2.3 ± 0.7	3 ± 0.7
NAF	4.4 ± 0.5	18 ± 3	3.1 ± 0.6	5 ± 1	4 ± 1	1.8 ± 0.6	5.1 ± 1.5

Table S2. Model calculation results for folding of the P2 and P3 hairpins. Predicted errors include the effects of uncertainties in the nearest-neighbor stacking parameters and in the value of the ssRNA persistence length.

Hairpin	**Δx (nm)**	**$F_{1/2}$ (pN)**	**$\Delta G^{\ddagger}$ (kcal/mol)**	**$\Delta x_f^{\ddagger}$ (nm)**	**$\Delta x_u^{\ddagger}$ (nm)**
P2	6.5 ± 0.4	6.9 ± 0.6	6.9 ± 0.5	2.2 ± 0.2	4.3 ± 0.4
P3	4.8 ± 0.4	6.7 ± 0.6	5.0 ± 0.4	1.4 ± 0.2	3.3 ± 0.4

References

S1. S. A. Darst, *Curr. Opin. Struct. Biol.***11,** 155 (2001).
S2. K. C .Neuman, E. A. Abbondanzieri, R. Landick, J. Gelles, S. M. Block, *Cell* **115**, 347 (2003).
S3. R. V. Dalal *et al.*, *Mol. Cell* **23**, 231 (2006).
S4. E. A. Abbondanzieri, W. J. Greenleaf, J. W. Shaevitz, R. Landick, S. M. Block, *Nature* **438**, 460 (2005).
S5. W. J. Greenleaf, M. T. Woodside, E. A. Abbondanzieri, S. M. Block, *Phys. Rev. Lett.* **95**, 208102 (2005).
S6. M. Mañosas *et al.*, *Biophys. J.* **92**, 3010 (2007).
S7. M. D. Wang, H. Yin, R. Landick, J. Gelles, S. M. Block, *Biophys. J.* **72**, 1335 (1997).
S8. Y. Seol, G. M. Skinner, K. Visscher, *Phys. Rev. Lett.* **93**, 118102 (2004).
S9. Y. Seol, G. M. Skinner, K. Visscher, *Phys. Rev. Lett.* **98**, 158103 (2007).
S10. F. Vanzi, Y. Takagi, H. Shuman, B. S. Cooperman, Y. E. Goldman , *Biophys. J.* **89**, 1909 (2005).
S11. P. Mangeol, D. Cote, T. Bizebard, O. Legrand, U. Bockelmann, *Eur. Phys. J. E* **19**, 311 (2006).
S12. G. Caliskan *et al.*, *Phys. Rev. Lett.* **95**, 268303 (2005).
S13. F. Kienberger *et al.*, *Biomaterials* **28**, 2403 (2007).
S14. W. Saenger, *Principles of Nucleic Acid Structure* (Springer, New York, 1984).
S15. M. T. Woodside *et al*., *Science* **314**, 1001 (2006).
S16. M. T. Woodside *et al.*, *Proc. Natl. Acad. Sci. USA* **103**, 6190 (2006).
S17. O. Dudko, G. Hummer, A. Szabo, *Phys. Rev. Lett.* **96**, 108101 (2006).
S18. C. Jarzynski, *Phys. Rev. Lett.* **78**, 2690 (1997).
S19. J. Gore, F. Ritort, C. Bustamante, *Proc. Natl. Acad. Sci. USA* **100**, 12564 (2003).
S20. J. K. Wickiser, M. T. Cheah, R. R. Breaker, D. M. Crothers, Biochemistry 44, 13404 (2005).
S21. S. Cocco, J. F. Marko, R. Monasson, *Eur. Phys. J. E Soft Matter* **10**, 153 (2003).
S22. C. Hyeon, D. Thirumalai, *Proc. Natl. Acad. Sci. USA* **102**, 6789-6794 (2005).
S23. J. R. Vieregg, I. Tinoco Jr., *Mol. Phys.* **104**, 1343 (2006).
S24. J. Liphardt, B. Onoa, S. B. Smith, I. Tinoco, Jr., C. Bustamante, *Science* **292**, 5517 (2001).
S25. R. T. Batey, S. D. Gilbert, R. K. Montange, *Nature* **432**, 411 (2004).
S26. A. Serganov *et al.*, *Chem. Biol.* **11**, 1729 (2004).
S27. C. Bustamante, Y. R. Chemla, N. R. Forde, D. Izhaky, *Annu. Rev. Biochem.* **73**, 705 (2004).
S28. O. M. Ottink *et al.*, *RNA* **13**,2202 (2007)
S29. J.-F. Lemay, J. C. Penedo, R. Tremblay, D. M. J. Lilley, D. A. Lafontaine, *Chem. Biol.* **13**, 857 (2006).